Wavelet-based multiscale analysis of bioimpedance data measured by electric cell-substrate impedance sensing for classification of cancerous and normal cells

Debanjan Das, Kumar Shiladitya, Karabi Biswas, and Pranab Kumar Dutta
Department of Electrical Engineering, IIT Kharagpur, India

Aditya Parekh, Mahitosh Mandal, and Soumen Das*
School of Medical Science and Technology, IIT Kharagpur, India

(Received 26 May 2015; revised manuscript received 12 October 2015; published 7 December 2015)

The paper presents a study to differentiate normal and cancerous cells using label-free bioimpedance signal measured by electric cell-substrate impedance sensing. The real-time-measured bioimpedance data of human breast cancer cells and human epithelial normal cells employs fluctuations of impedance value due to cellular micromotions resulting from dynamic structural rearrangement of membrane protrusions under nonagitated condition. Here, a wavelet-based multiscale quantitative analysis technique has been applied to analyze the fluctuations in bioimpedance. The study demonstrates a method to classify cancerous and normal cells from the signature of their impedance fluctuations. The fluctuations associated with cellular micromotion are quantified in terms of cellular energy, cellular power dissipation, and cellular moments. The cellular energy and power dissipation are found higher for cancerous cells associated with higher micromotions in cancer cells. The initial study suggests that proposed wavelet-based quantitative technique promises to be an effective method to analyze real-time bioimpedance signal for distinguishing cancer and normal cells.

DOI: 10.1103/PhysRevE.92.062702 PACS number(s): 87.80.−y, 05.40.−a, 87.90.+y

I. INTRODUCTION

In vitro real-time and continuous monitoring of cell growth, proliferation, and cell viability is crucial to biological research to understand the complicated pathways regulating proliferation and viability, and to develop agents that modulate these processes. In addition, a detail kinetic behavior of cells provides important information about the biological state of the cell, revealing, for example, enhanced cell growth, cell quiescence, morphological changes, or cell death, especially in the field of cancer biology. It has been well established that the growth kinetics of cancer cells is distinguishably different from that of normal cells [1]. Traditionally, the cell growth and proliferation are observed through *in vitro* cell culture system using different microscopic techniques. Nevertheless, it has been still a challenge to monitor real-time cellular behavior through available techniques. Recently, electric cell-substrate impedance sensing (ECIS) based on impedance spectroscopy has been widely used to continuously monitor cell culture and growth dynamics [2,3]. ECIS has been mostly exploited for electrical characterization of growing cells along with quantitative information about cell adhesion [3], growth kinetics [4], migration [5], apoptosis [6], and morphological changes, etc. ECIS has been successfully demonstrated to characterize cancer and normal cells through the measurement of overall impedance of a cell layer at various frequencies at a particular time instance and by subsequent modeling of electrical equivalent circuit. It has been found that monitoring of real-time growth dynamics at *in vitro* model is worthwhile for understanding of complex behavior of cancer cells in comparison to normal cells like dynamic cell viability, migration, and invasion [7,8]. Since ECIS can monitor cell growth, spreading during cell culture in terms of bioimpedance value, which varies with cell types, it will be more advantageous to establish the distinguishing features by considering the entire growth kinetics of cell cycle. It has been observed that real-time impedance measurement signals are always associated with fluctuations. Impedance variations in cell-cell and cell-substrate gap associated with cellular level interaction and their signal transduction appears as the fluctuations in the recorded bioimpedance data. Some groups [9–12] have reported that these impedance fluctuations are directly correlated with cellular micromotions, which differ for cancerous and normal cells. Micromotions are the result of micromovements in the cell membrane protrusions mainly required during cell migration and invasion but are also produced during other vital processes, like cell division. The present study assumed the micromotions stemmed from dynamic structural rearrangement of filopodia, lamellipodia, or membrane ruffles in micrometer scale. Cellular extensions like filopodia and lamellipodia are required for sensing the chemoattractant in cellular environment, cell adhesion, detachment, and cell-cell communication [13]. Elongation, retraction, and dynamic changes in these structures are also required for cellular migration, invasion, and interaction with matrix [14,15]. Through this extension the cell attaches to the matrix surface followed by the contraction of the whole cell body and leaving the earlier attachments. The movement through pseudopods (lamellopodia, filipodia, and podosomes being its different types) is actually mediated by the network of actins (i.e., cytoskeleton), which periodically contracts and relaxes to mediate movement in a particular direction by intricate and defined cellular signaling [16]. These protrusive and chemotactic movements are moreover found during *in vivo* cell migration and more importantly during invasion of cancer cells through blood capillaries to undergo distant metastasis, whereby cancer spreads and disseminates throughout the body [17]. This rearrangement of cell membrane protrusions results in oscillation of membrane structure, which

*Corresponding author: sou@smst.iitkgp.ernet.in

is required for cellular migration, invasion, and interaction with matrix and other cells [14,18]. Although in the structural rearrangement event the amplitude of micromotion is at the micron level, the reorientation of the cellular structure occurs at μm/min velocity [19,20]. Therefore, the study of micromotion is an important aspect in cancer biology as it provides the information about cell motility and its response to various external stimuli. Cancer cells have a unique kind of intercellular and intracellular interactions due to their uncontrolled and unregulated division and associated metabolic processes. This leads to their differences in motility as well as in their response to external chemical signals leading to difference in their micromotions with noncancerous cells. Thus, the analysis of micromotion reflected on bioimpedance fluctuation could be an important characteristic to study the growth kinetics of cancer and normal cells. Numerous techniques have been explored to study these bioimpedance fluctuations for understanding the cellular property. For example, D.C. Lovelady *et al.* had established a statistical technique to study the electrical noise in bioimpedance signal in order to distinguish cancer cells from normal cells [10]. They have used Hurst exponent and detrended fluctuation analysis (DFA) to study the long-term correlation of noisy signal. Marimuthu *et al.* [12] demonstrated a correlation between oscillatory motion of cells with the impedance change through FFT analysis. Tarantola *et al.* [21] used Fourier transform to analyze the dynamics of human cancer cell lines monitored by electrical and acoustic fluctuation analysis. Short-time Fourier transform (STFT) is used by Wang *et al.* [22] to distinguish three different normal cells. However, Fourier transform is not effective for nonstationary type bioimpedance signal, since the moment it transforms the signal into frequency domain the time information is lost. Although the STFT overcomes the time location problem to a large extent, it does not provide multiple resolution in time and frequency, which is an important characteristic for analyzing transient signals containing both high- and low-frequency components. Wavelet analysis overcomes the limitations of Fourier transform and STFT method by employing the analyzing functions that are available locally both in time and frequency domain. Yi-Ting Lai *et al.* used Hilbert-Huang transform (HHT) [23] to study the cytotoxicity effect on cell micromotion of endothelial cells. Recently, Chen *et al.* group [24] has applied wavelet transform to quantify the fluctuations associated with fibroblast cell (3T3) micromotions. Although wavelet has been widely applied on different biological signals (mostly ECG and EEG signal), its application to the bioimpedance signal for classification of cells is largely unexplored area. To the authors knowledge, until now there has been no study of wavelet-based characterization of micromotion of cancer cells. The wavelet transform can decipher the detail information through layer-by-layer filtering of high-frequency and low-frequency components of the signal. Thus, the wavelet transform can be described as a mathematical microscope, allowing one to provide detailed information of the signal with multiscale observational facility. The main advantage of wavelets, like in doing multiscale analysis or choosing different kinds of wavelets for different analyses, suggests that it could be very well suited for the study of bioimpedance signal.

In this work, real-time impedance during cell culture of human breast cancer cells (MCF-7 and MDA-MB-231) and human epithelial normal cells (HaCaT) was measured using ECIS-based technique. Subsequently, discrete wavelet transform (DWT)-based data analysis technique has been established first time to investigate the time-series bioimpedance data. The proposed technique was demonstrated to distinguish cancerous cells from normal cells. DWT has been applied on the temporal impedance data to decompose the signal into high-pass and low-pass filter outputs called approximation and detail, respectively, in four levels. The high-frequency component is directly related with the micromotion of the cells. In the present study, three novel parameters, "cellular energy," "cellular power," and "cellular moments" have been introduced to characterize the detail and approximate signals. The different biological activities during cell growth, confluence, and death phase of cells can be mapped with these parameters. In the growing and confluence phase, cells start to migrate, interact with neighbor cells, respectively, via movement of lamellipodia and filopodia, which involve dynamic changes in the structure of actin filaments. This requires presence of substantial amount of energy inside the cells to induce and retract the cellular protrusions. Thus, the enhanced capability of cell-cell interactions and migrations properties of cells can be correlated with the kinetic energy of the cells to have more filament movement involved in cell micromotions, resulting in impedance fluctuations. Further, rate of work done to move the filament can be correlated with total power loss during a full cycle of filament movement. Here, the energy and power dissipation due to cellular movement of the detail signal at four decomposition levels are calculated and defined as "cellular energy" and "cellular power," respectively. These provide a quantitative measures of cellular micromotions. Furthermore, first-, second-, and third-order moments defined as "cellular moments" of the approximate signals were computed. The present study demonstrates an alternate technique to classify cancer and normal cells by monitoring and analyzing real-time bioimpedance data and intends to measure overall dynamics of cellular projections like lamellipodia and filopodia without directly measuring their differences in morphology and migration. Here, it has been found that cellular-energy, cellular-power, and cellular-moments associated with micromotions differ significantly for cancerous and normal cells and, subsequently, these parameters are established as signature for classification of cancerous and normal cells.

II. MATERIALS AND METHOD

A. Cell line and cell culture on ECIS device

Normal human epithelial cells (HaCaT cells) and two types of human breast cancer cells (MCF-7 and MDA-MB-231) were cultured in culture medium composed of Dulbecco's modified Eagle's medium (DMEM) containing 10% fetal bovine serum (FBS), 1% penicillin, and 100 μg/ml streptomycin and maintained in a humidified incubator at 37°C and 5% CO_2. Once confluence was achieved, cells were removed from flask surface by trypsinizing the cells with 0.05% trypsin/EDTA. Subsequently, cells were resuspended in fresh DMEM medium and 400 μl of cell suspension was added to ECIS well. The

device was placed in that same incubator and connected to an impedance analyzer to measure the impedance value.

B. Impedance measurement

An ECIS-8W1E DD (Applied BioPhysics, USA) cell culture well was used to measure the bioimpedance. At first, the ECIS culture wells were sterilized by UV treatment and cells were seeded inside the well. The ECIS device consists of eight separate mini-culture wells having an individual working electrode (WE) and common counter electrode (CE). The top surface of each working electrode was coated with a thin biocompatible polymer with a circular opening of 250-μm diameter at its center. Counter and working electrodes were connected to an impedance analyzer (HIOKI LCR-3532) interfaced with a computer. The present study focused on monitoring the micromotions resulting in changes of cell membrane protrusions. These changes require active remodeling of the intracellular cytoskeletal protein actin, and several other actin-associated proteins. Through numerical simulation it has been found that at 40 kHz the electric field lines are distributed in the entire cell-layer, including both intra- and intercellular pathway. Thus, to capture overall changes in membrane protrusions resulting from variation in intracellular dynamics of cytoskeletal proteins, impedance value of growing cells was measured in real time at 40-kHz frequency with excitation voltage of 10 mV. Moreover, a customized experimental setup consisting of fast-switching circuit and software was developed to explore the dynamic events during the entire cell-growth period (60–90 h) in real time with avoiding the direct continuous intervention of external electric field, which may alter the natural cellular activities. It has also been reported that the micromotions originated from continuous rearrangement of cellular protrusions and intracellular mass movement for cell-cell interaction and migration [18]. Although the amplitude of structural reorganization is in the submicron level, the rearrangement of cell body is a time-driven phenomena and persist for several minutes [19]. Therefore, in the present study data were acquired throughout the experiment without changing the culture medium at an interval of 5 min till the cells were dead after reaching 100% confluence. Initially, 400 μl of DMEM medium was poured and impedance value was measured as same procedure for 30 min. The average of these impedance values of fresh medium was used for baseline correction. Subsequently, medium was replaced with cells suspended in the same volume of fresh medium and measurements were repeated. The present study is aimed to classify cancer and normal cells through measurement of real-time growth kinetics during cell culture considering micromotion as a marker. To achieve micromotion for cell-cell communication, formation of monolayer is essential within a stipulated time. Since the growth kinetics of HaCaT cells is very slow at a lower cell concentration because of its epithelial nature as compared to cancer cells (MCF-7 and MDA-MB-231), a little higher concentration of HaCaT cells was taken during experiment to form a complete monolayer and sheetlike structure. All the experiments were performed three times and the average impedance values were taken. As cells grow on the electrodes, there is change in impedance across the two electrodes, which is recorded by impedance analyzer. Finally, the measured impedance values of different cells were generalized as differential-normalized impedance (Z_N) with respect to the initial measured impedance value of medium according to Eq. (1).

$$Z_N = \left(\frac{Z_c - Z_m}{Z_m}\right), \tag{1}$$

where Z_m and Z_c are impedance of medium only and medium with cells, respectively.

C. DWT-based multiresolution analysis (MRA)

The wavelet transform becomes a powerful analyzing tool for stationary, nonstationary, intermittent time series, especially, to find out hidden short events inside the time series [25]. The advantages of wavelets are that they are able to represent a signal in the time and frequency domain at the same time leading to handle of wider range of signals than Fourier analysis. A wavelet is a function $\psi \in L^2(R)$ with a zero average [26]; i.e.,

$$\int_{-\infty}^{+\infty} \psi(t)dt = 0. \tag{2}$$

The DWT of a signal is defined as

$$W(j,k) = \frac{1}{\sqrt{2^j}} \int_{-\infty}^{+\infty} x(t)\psi^*\left(\frac{t - k2^j}{2^j}\right)dt, \tag{3}$$

where $\psi(t)$ is called the mother wavelet, ψ^* represents the complex conjugate of the mother wavelet, the dyadic sequence 2^j is the scaling parameter, and $k2^j$ denotes the translation parameter. The sampled dyadic scale parameter determines the oscillatory frequency and length of wavelet, and the translation parameter determines its shifting position. DWT consists of two sets of functions called scaling function $\phi_{j,k}(t)$ and the wavelet function $\psi_{j,k}(t)$, which are defined as follows:

$$\phi_{j,k}(t) = 2^{-\frac{j}{2}}\phi(2^{-j}t - k), \psi_{j,k}(t) = 2^{-\frac{j}{2}}\psi(2^{-j}t - k), \tag{4}$$

where j,k are integers. DWT decomposes a time series signal into the approximations coefficients ($A_{j,k}$) and the detail coefficients ($D_{j,k}$) provided by scaling function associated with low-pass filter (LPF) and wavelet function associated with high-pass filter (HPF), respectively. The approximation coefficient is split again into high- and low-frequency components to get multiresolution decomposition of a signal, which is shown schematically in Fig. 1.

The output of these filters are given by

$$A_{j,k} = \sum_n l(n - 2k)a_{j-1,n}, D_{j,k} = \sum_n h(n - 2k)a_{j-1,n}, \tag{5}$$

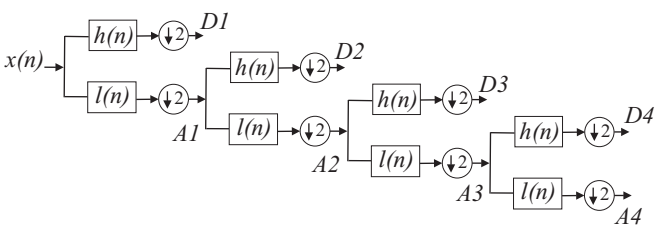

FIG. 1. DWT-based decomposition process of a signal $x(n)$.

where $l(n)$ and $h(n)$ are the filter coefficients of LPF and HPF, respectively. The number of decomposition levels is selected based on the dominant frequency components of the signal. In this study, the measured time-series impedance data is decomposed up to four levels having approximations $A1$–$A4$ and details $D1$–$D4$. Since the temporal resolution is better for Daubechies 8 (Db8), the mother wavelet Db8 has been chosen for the present analysis of bioimpedance signals.

D. Cell features in terms of wavelet

The extracted wavelet coefficients provide a compact representation that shows the energy distribution of the signal in time and frequency. The following features were computed and used to represent the time-frequency distribution of the bioimpedance signals:

1. Cellular-energy: Signature of wavelet coefficient energy

The different levels of wavelet coefficients over the scales can be interpreted as uneven distribution of energy across the multiple frequency bands. This distribution pattern has been found to be useful for classifying between different cells. According to Parseval's theorem, the energy of the signal can be partitioned at different resolution levels. In conjunction with the definition of signal energy, the wavelet coefficient energy at the jth level for n number of samples, denoted as E_j, can be calculated by Eq. (6),

$$E_j = \sum_{n=1}^{N_j} D_j^2(n), \tag{6}$$

where N_j is the length of detailed signal $D_j(n)$. In the present work, the wavelet coefficient energy is introduced as "cellular-energy." The cellular energy provides direct quantitative information of the energy of the living cells to execute the physiological and biological activities. In this work, the "cellular energy" of all three types of cells are computed for four different levels ($D1$–$D4$).

2. Cellular power: Signature of wavelet coefficient power

In time-series bioimpedance signal, each detail signal can be represented as being the fluctuation associated with the cell micromotion. In order to estimate the level of fluctuation, the power dissipation due to cellular micromotion can be calculated. The power dissipation in each decomposition level of the detail signal due to current I is termed as "cellular power" according to Eq. (7):

$$P_j = \left(\sqrt{\frac{1}{N_j} \sum_{n=1}^{N_j} D_j^2(n)} \right) I^2. \tag{7}$$

3. Cellular moments: Signature of wavelet coefficient moment

Moment calculation is standard approach in statistics to get an insight about a distribution, such as spread, dispersion, and shape of the distribution. Since it is believed that growth pattern of normal and cancerous cells differ significantly, the moment calculation of their bioimpedance signal has been done to determine difference based on these statistical parameters. The nth moment of a real-valued continuous function $f(x)$ of a real variable about a value "a" is given by Eq. (8):

$$\mu_n = \int_{-\infty}^{+\infty} (x-a)^n f(x) dx. \tag{8}$$

In this work, the moment of each approximate signal ($A1$–$A4$) was calculated and termed as "cellular moments." The first-order raw moment is mean, while second-order central moment gives variance. The value of "a" is zero for the calculation of mean and variance. Mean and variance provide information on the location and variability (spread, dispersion) of a set of numbers, and by doing so, provide some information on the appearance of the distribution of the numbers. The third-order central moment gives skewness of the data set. The skewness describes the distribution of the signal, i.e., whether the mass of distribution is concentrated on the right side or left side. Thus, skewness gives a quantitative information about growth rate of cell.

III. RESULTS AND DISCUSSION

A. Real time bioimpedance-based cell-growth monitoring

The impedance value of growing cells was measured in real time at an interval of 5 min at 40 kHz frequency. As cells start attaching to the bottom electrodes, the current flow alters between the counter and working electrodes resulting in increased impedance value. Figures 2(a), 2(b), and 2(c) show the real-time growth kinetics of HaCaT, MCF-7, and MDA-MB-231 cells in terms of bioimpedance signal, respectively. All the experiments were conducted three times and the average of them was plotted in Fig. 2.

A typical bioimpedance signal has different phases of cell-growth kinetics, i.e., proliferation, confluence, and death, clearly morphed in increase and decrease of magnitude of bioimpedance signal. Figure 2 describes the different phases of cell-growth kinetics as follows:

(i) Cell growth: When cells are inoculated in the wells initially they attach on the surface and then they start to spread on the electrode area, which is followed by cell division. This leads to increase in impedance of the electrode due to area coverage by cells. Thus, in the first phase of cell growth, the bioimpedance value increases proportionately as cells grow, spread, and divide.

(ii) Confluence phase: As cells start growing and dividing, they become confluent and in the process cover the maximum surface area, which gives rise to maximum and nearly constant impedance value. The value remains nearly constant with minimum variation till cell death is activated.

(iii) Death phase: Due to lack of space and nutrient availability with time, cells switch to death mode by undergoing apoptosis. As cells start to die they start losing cell-cell as well as cell-substrate adhesion, which eventually leads to decrease in bioimpedance.

From Fig. 2 it can be observed that the growth rate of cancer cells is faster (higher rising slope) than that of normal cells. Further, Fig. 2 also depicts that the measured time-series bioimpedance signals consist of small fluctuations. These fluctuations are associated with the micromotion of cells resulting in a minor change in current pathways, which ultimately leads to oscillation in measured bioimpedance.

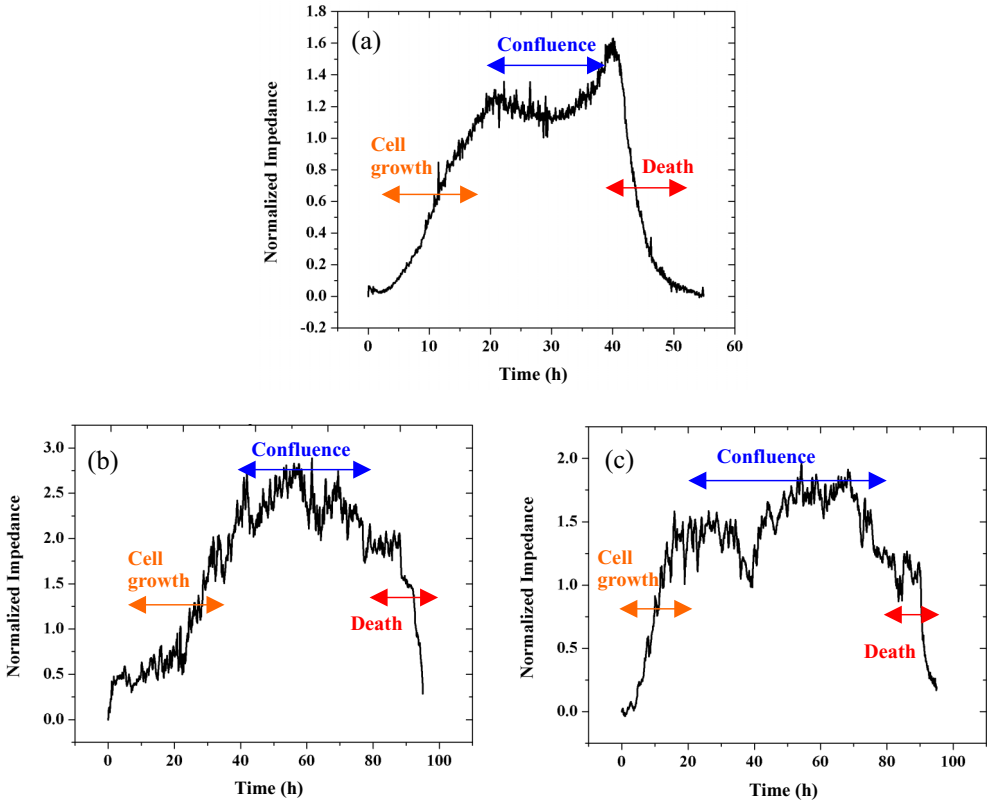

FIG. 2. (Color online) Time-course impedance measured on an ECIS sensing device during the cell culture of (a) HaCaT (normal cells), (b) MCF-7 (breast cancer cells), and (c) MDA-MB-231 (breast cancer cells) at 40 kHz.

The micromotion associated with overall dynamic structural rearrangement of filopodia, lamellipodia, or membrane ruffles in micrometer scale. Figure 3 shows the phase contrast images along with membrane protrusions of HaCaT, MCF-7, and MDA-MB-231 cells at their maximum confluence stage. The MCF-7 and MDA-MB-231 breast cancer cells have prominent structures like filopodia as depicted from Fig. 3. Although MDA-MB-231 cells had larger and prominent filopodia, MCF-7 cells revealed more such structures but smaller and less distinguished. Whereas HaCaT cells have the least prominent filopodia and lamellipodial structures, they thus form a well-defined monolayer in culture plate. This indicates that micromotions originated from these dynamic arrangement and rearrangement of these cellular projections should differ for cancer cells. This is also revealed from Fig. 2, which describes that impedance fluctuations correlated to cellular micromotion is different for normal cells (HaCaT) and cancer cells (MCF-7, MDA-MB-231). Thus, the study of micromotion will help understanding cellular migrations cell-cell communication, cell motility, etc. Since the different types of cells will have different kinds of intercellular and intracellular interactions, their motility is bound to differ. Therefore, the micromotion could be an important aspect of study of cell-growth kinetics for distinguishing different types of cells. The bioimpedance-based study could successfully describe the detailed growth kinetics of normal and cancer cells, which was further used to distinguish the cancerous cells from normal cells.

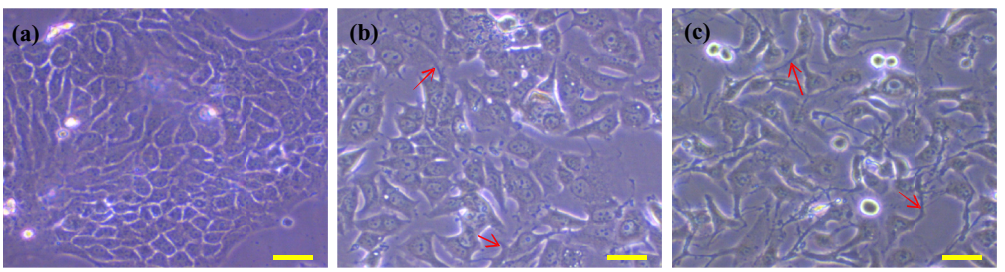

FIG. 3. (Color online) Phase contrast microphotograph during their confluence stage for (a) HaCaT, (b) MCF-7, and (c) MDA-MB-231 cells. Red arrow indicates the membrane protrusions, filopodia. MDA-MB-231 cells had larger and prominent filopodia, and MCF-7 cells revealed more such structures but smaller and less distinguished, whereas it is least prominent in HaCaT. Scale bar $= 50\,\mu$m.

B. DWT-based analysis of bioimpedance signal

In this study, DWT has been used to analyze these bioimpedance signals in depth and to find distinguishing characteristics features. A four-level DWT-based multiscale analysis using the Db8 wavelets has been performed to decompose the bioimpedance value of cancer and normal cells as shown in Fig. 4. The wavelet coefficients, as shown in the right panels in Fig. 4, provide the detail characteristics. The variation of approximation and detail in Fig. 4 shows that at the beginning when value of bioimpedance is low, the fluctuation of detail coefficient is also low, correlating with initial start of cell growth. In the first few hours cells start to attach and attain its shape maintaining less cellular micromotion. While the number of cells was increasing due to cell division and proliferation, the level of fluctuation due to cell micromotion in each band was getting higher, thus consistently agreeing to a hypothesis that the greater the number of living cells, the higher the level of fluctuation. Furthermore, when cells become confluent it still continues its cellular movement for signal transduction. Therefore, impedance fluctuation in detail is observed throughout this confluence phase. Finally, when cells enter in death phase, cell micromotion is ceased, which can also be observed from decaying oscillations in the detail signal. It can be easily observed that there is a distinguishable difference in cellular micromotion for cancerous (MCF-7 and MDA-MB-231) and normal cells (HaCaT). Figure 4 depicts that impedance fluctuation for cancer cells is more throughout the times. MDA-MB-231 cells (basal type) have been reported to be more invasive and having greater migratory potential than MCF-7 cells (luminal type) [27]. Therefore, during the growth of cancer cells and while cells reach confluence in a two-dimensional culture plate, they tend to migrate and interact with other cells with the help of cellular protrusions apart from undergoing cellular division. HaCaT, on the other hand, is an immortalized keratinocyte having minimal cellular protrusions like filopodia, and forms a regular-colonies, tight sheetlike structure with strong cell-cell adhesions, least migratory potential, and no invading characteristics [28]. The detail subfigures in Fig. 4 also describe that cancer cells continue the impedance fluctuations even in death phase compare to normal cells. Therefore, in the present study, the cellular micromotion is considered as a main parameter to classify cancerous and normal cells. To achieve the goal, the different features of the detail wavelets ($D1$–$D4$) are calculated for each type of cells.

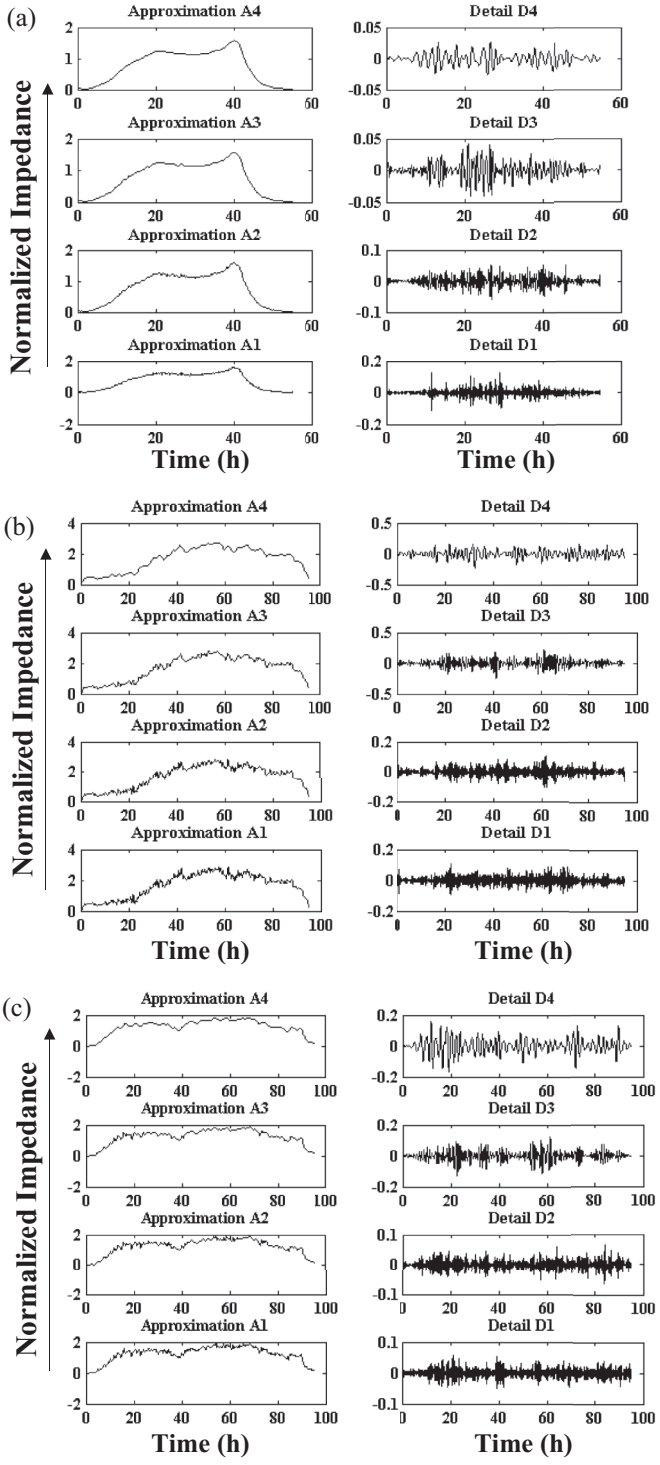

FIG. 4. Wavelet decomposition results of bioimpedance signal using Db8 for (a) HaCaT, (b) MCF-7, and (c) MDA-MB-231 cells.

C. Correlation between cell types and wavelet features

The energy, power, and moment of each of the detail and approximate signal were calculated, which showed a good correlation with cell types, e.g., cancerous and normal cells. The signal processing and statistical parameters were established as the quantitative signatures to distinguish cancerous and normal cells.

1. Cellular-energy analysis

Wavelet energy provides a good indication of the total energy contained at a specific spatial frequency level. Here, the energy of the detail signals at all four levels ($D1$–$D4$) was calculated for all three cells based on Eq. (6), which is the sum of the instantaneous energy over the total time cycle of cell growth. Table I summarizes the cellular energy values of normal (HaCaT) and breast cancer (MCF-7, MDA-MB-231) cells. It can be observed from Table I that the "cellular-energy" values at third and fourth level, i.e., ($D3\_E$) and ($D4\_E$) for MCF-7 and MDA-MB-231 cells have distinguishably higher than that of HaCaT cells. Here, micromotion represents overall dynamic changes in lamellipodia and filopodia involving in

TABLE I. Energy obtained from detail coefficients for HaCaT, MCF-7, and MDA-MB-231 cells.

Features	Parameter	HaCaT	MCF-7	MDA-MB-231
	$D1\_E$	0.383 ± 0.019	0.724 ± 0.058	0.232 ± 0.011
Cellular	$D2\_E$	0.172 ± 0.013	0.785 ± 0.0314	0.285 ± 0.014
energy	$D3\_E$	0.087 ± 0.004	3.48 ± 0.02	1.06 ± 0.084
(a.u.)	$D4\_E$	0.051 ± 0.004	3.93 ± 0.117	2.47 ± 0.074
Cellular	$D1\_P$	2.41 ± 0.096	2.52 ± 0.10	1.43 ± 0.057
power	$D2\_P$	1.62 ± 0.081	2.62 ± 0.157	1.58 ± 0.126
(a.u.)	$D3\_P$	1.15 ± 0.080	5.52 ± 0.110	3.05 ± 0.061
$\times 10^{-14}$	$D4\_P$	0.886 ± 0.026	5.87 ± 0.117	4.65 ± 0.139

continuous rearrangement of actin filaments in association with several actin-associated proteins and GTP as energy source [29,30], which has a leading role to play in cancer cell migration and invasion. Thus, huge mechanical forces are generated through molecular changes in cellular cytoskeleton to induce and retract the formed cellular protrusions, which are very important for cellular tethering to its surface and directional movement [20]. The measured energy of the signal involves cell energy expenditure as stated above, which may be correlated directly with the calculated energy of detail coefficients. The energy at different level decomposition can be correlated with short-term and long-term disturbances. The "cellular-energy" value of normal cells reduces with increase of level of decomposition. This infers that the normal cells have more short-term disturbance, while cancer cells express long-term disturbance. Here, $D4\_E$ (cellular energy at the fourth level) is most significant in terms of long-term disturbance and subsequently used as classifier to characterize cancer and normal cells. The energy can be physically described as the work capacity accumulated during its deformation to the final relief. Normal HaCaT cell forms an epithelial layer *in vitro* [28] and displays little cellular migration potential. MCF-7 although being a cancerous cell line is much more adhesive in nature with lesser invasive and migratory potential. MDA-MB-231 nevertheless has over-expression of those proteins, which are involved in invasion and metastasis, with minimum or no ability to form a single epithelial layer *in vitro* [31]. Thus, the highly metastatic and invasiveness potential of cancer cells increases the overall work capacity correlating with micromotion. Moreover, it is also found that cancer cells escape from cellular senescence and become immortal by activating telomerase [32]. This activation of telomerase keeps the cancer cells in the long-term proliferation stage, which leads to increase in the cellular activities. Further, cellular-energy $D3\_E$, $D4\_E$ of all three cells were calculated at different phases of cell growth as summarized in Table II. The results show that energy value during growth and confluence phases is higher than that of death phase. This observation infers that cells are more active in the first two phases. Moreover, the amount of energy carried by a signal is directly related to the amplitude of the signal. A high-energy signal is characterized by a high amplitude, while a low-energy signal is characterized by a low amplitude with signal duration maintaining same. The amplitude of a signal refers to the maximum amount of displacement from its rest position. The cellular energy was calculated without padding any additional data points to obtain the original information based on Eq. (6), which is dependent on time length. Further, the cellular-energy $D3\_E$, $D4\_E$ of all three cells have been calculated with respect to the same time interval (10 h), irrespective of total time duration at three growth phases to support the results. The calculated results are shown in Table III, which again depicts that cancerous cells have higher "cellular energy" compared to normal cells, suggesting that cancerous cells have higher displacement, which is related to higher cellular micromotion of cancer cells. Thus, the energy of detail coefficients suggests that cancerous cells are more active and have higher micromotion than the other normal cells even under nonagitated condition. Hence, this "cellular-energy" feature can be used to distinguish between normal and cancer cells.

2. Cellular-power analysis

Here, cellular power provides the quantitative information about the power dissipation due to cellular micromotion. During the impedance measurement of cells typically 1 μA current is passed through the ECIS system. Thus, the power dissipation

TABLE II. Energy of detail coefficient ($D3\_E$ and $D4\_E$) at different phases for HaCaT, MCF-7, and MDA-MB-231 cells.

Phase	Parameter	HaCaT	MCF-7	MDA-MB-231
Growth	$D3\_E$	0.019 ± 0.0013	1.523 ± 0.076	0.088 ± 0.004
Phase	$D4\_E$	0.018 ± 0.0013	1.714 ± 0.068	0.608 ± 0.024
Confluence	$D3\_E$	0.058 ± 0.004	1.616 ± 0.080	0.841 ± 0.042
Phase	$D4\_E$	0.023 ± 0.001	1.5394 ± 0.061	0.975 ± 0.039
Death	$D3\_E$	0.009 ± 0.0001	0.334 ± 0.017	0.150 ± 0.007
Phase	$D4\_E$	0.013 ± 0.0002	0.728 ± 0.029	0.616 ± 0.024

TABLE III. Comparison of piecewise cellular energy ($D3\_E$ and $D4\_E$) for 10 h at different phases of cell growth for HaCaT, MCF-7, and MDA-MB-231.

Phase (10 h)	Parameter	HaCaT	MCF-7	MDA-MB-231
Growth	$D3\_E$	0.013 ± 0.0010	0.378 ± 0.019	0.083 ± 0.003
Phase	$D4\_E$	0.016 ± 0.0009	0.779 ± 0.023	0.298 ± 0.006
Confluence	$D3\_E$	0.029 ± 0.0017	0.336 ± 0.007	0.106 ± 0.005
Phase	$D4\_E$	0.011 ± 0.0008	0.252 ± 0.010	0.129 ± 0.004
Death	$D3\_E$	0.006 ± 0.0005	0.139 ± 0.007	0.062 ± 0.003
Phase	$D4\_E$	0.012 ± 0.0007	0.256 ± 0.010	0.117 ± 0.002

at each level of the detail coefficient is calculated based on Eq. (7) and the values are summarized in Table I. Since the power dissipation is a measure of the rate at which energy is dissipated or lost, higher cell-power dissipation reflects the work due to higher level of cellular micromotion. In this study, cell-power dissipation at the fourth level decomposition ($D4\_P$) was selected as a classifier that simply reflects the work due to long-term cellular micromotion. It was found that both the breast cancer cells MCF-7 and MDA-MB-231 showed comparatively higher cell-power dissipation than that of normal HaCaT cells. Thus, cancerous and normal cells can be successfully distinguished by measuring "cellular-power" dissipation of bioimpedance data.

3. Cellular-moments analysis

It has been seen that growth pattern of normal and cancerous cells differ, so the moment calculation of their bioimpedance signal has been done in order to see any difference based on these statistical calculations. The first-, second-, and third-order moments of each approximate signal ($A1$–$A4$) are calculated based on Eq. (8) for all three cells and the results are tabulated in Table IV. It was found that the mean of approximate signal ($M1\_A$) of MCF-7 and MDA-MB-231 cells is higher than HaCaT signifying that normalized impedance value of cancer cells is higher than that of normal cells. Furthermore, the higher value of variance ($M2\_A$) indicates that the distribution of impedance value of MCF-7 is more scattered, which can be correlated with more impedance fluctuation due to higher cellular movement. In general, the variance is equivalent to power of the signal. This analysis again supports the above finding higher "cellular-energy" and "cellular-power" dissipation of MCF-7 cells. The third-order central moment, skewness ($M3\_A$) is a measure of lopsidedness of the distribution of a time-series signal. The higher skewness values (with negative sign) of MCF-7 and MDA-MB-231 cells indicates that the mass of distribution is centered toward the right-hand side. Computing this feature from Fig. 2, the initial analysis shows that cell confluence and death phase of cancer cells were higher than that of HaCaT. Therefore, "cellular moments" can also be important features to characterize the cancer and normal cells based on their impedance-measured cell-growth kinetic.

IV. CONCLUSION

In this study, a wavelet-based multiscale analysis technique has been established to study the ECIS-captured bioimpedance data. The impedance associated with cell growth is monitored over time using an ECIS device. The measured real-time impedance signals are associated with fluctuations that reflect the fine changes in cellular behavior and movement. Thus, a quantitative analysis technique is demonstrated to study the cellular dynamics. When cells are transformed from normal to malignancy stage cellular dynamics, cell-body structure, membrane projections, and behavior changes markedly, which leads to change in their micromotions. Here, the micromotions are assumed to originate from dynamic structural rearrangement of filopodia, lamellipodia, or membrane ruffles in micrometer

TABLE IV. Moments obtained from approximation values for HaCaT, MCF-7, and MDA-MB-231 cells.

Moments	Parameter	HaCaT	MCF-7	MDA-MB-231
First order	$M1\_A1$	0.758 ± 0.017	1.665 ± 0.033	1.245 ± 0.012
(mean)	$M1\_A2$	0.758 ± 0.007	1.665 ± 0.041	1.245 ± 0.025
	$M1\_A3$	0.758 ± 0.022	1.665 ± 0.049	1.245 ± 0.037
	$M1\_A4$	0.758 ± 0.011	1.666 ± 0.017	1.245 ± 0.012
Second order	$M2\_A1$	0.262 ± 0.013	0.609 ± 0.030	0.235 ± 0.012
(variance)	$M2\_A2$	0.261 ± 0.013	0.608 ± 0.0304	0.233 ± 0.009
	$M2\_A3$	0.261 ± 0.013	0.605 ± 0.0302	0.233 ± 0.014
	$M2\_A4$	0.262 ± 0.013	0.601 ± 0.030	0.231 ± 0.011
Third order	$M3\_A1$	−0.032 ± 0.0016	−0.213 ± 0.008	−0.131 ± 0.006
(skewness)	$M3\_A2$	−0.032 ± 0.0019	−0.213 ± 0.010	−0.131 ± 0.005
	$M3\_A3$	−0.033 ± 0.0013	−0.215 ± 0.013	−0.132 ± 0.008
	$M3\_A4$	−0.033 ± 0.0023	−0.216 ± 0.006	−0.132 ± 0.003

scale. A four-level DWT-based multiscale analysis using the Db8 wavelets has been performed to decompose the bioimpedance values, subsequently the approximation and detail coefficients are further analyzed. It has found that the detail coefficients are directly correlated with cellular micromotion. Subsequently, in this study, three novel parameters—cellular energy, cellular power, and cellular moments—have been introduced to characterize and distinguish human breast cancer cells (MCF-7, MDA-MB-231) and normal epithelial cells (HaCaT). The cellular energy and cellular power provide a quantitative information of intensity of impedance fluctuations associated with cellular micromotion. Cellular-energy and cellular-power dissipation may be correlated with associated biological activities to alter the cell-body projections through molecular changes in cellular cytoskeleton. The results indicate that cancerous cells have higher "cellular energy" compared to normal cells, suggesting that cancerous cells are more active and have higher cellular displacement. It is also revealed that cellular-power dissipation due to its micromovement is higher for MCF-7 and MDA-MB-231 cells. Further, the first-, second-, and third-order moments of each approximate signal ($A1$–$A4$) termed as "cellular moments" describes the magnitude, distribution, and variation of impedance value coupled with cell-growth kinetics. These results indicate that the proposed wavelet-based technique promises to be an effective tool for characterization and differentiating cell types with the capability to measure overall dynamics of cellular projections like lamellipodia and filopodia, avoiding direct monitoring of their differences in morphology and migration. Following technique may further be explored on other sets of cancer and normal cell lines to validate these results and consider its translational value in formulating diagnostic tool.

ACKNOWLEDGMENTS

The authors acknowledge MEMS Lab in ATDC, IIT Kharagpur, for the necessary support. The authors also thank the Cancer Biology Lab at the School of Medical Science and Technology, IIT Kharagpur, for providing the cell line and laboratory facility to conduct the experiment.

[1] M. J. Bissell, Int. Rev. Cytol. **70**, 27 (1981).
[2] Y. A. Abassi, B. Xi, W. Zhang, P. Ye, S. L. Kirstein, M. R. Gaylord, S. C. Feinstein, X. Wang, and X. Xu, Chem. Biol. **16**, 712 (2009).
[3] J. Wegener, C. R. Keese, and I. Giaever, Exp. Cell Res. **259**, 158 (2000).
[4] J. H. T. Luong, M. Habibi-Rezaei, J. Meghrous, C. Xiao, K. B. Male, and A. Kamen, Anal. Chem. **73**, 1844 (2001).
[5] C. R. Keese, J. Wegener, S. R. Walker, and I. Giaever, Proc. Natl. Acad. Sci. USA **101**, 1554 (2004).
[6] S. Arndt, J. Seebach, K. Psathaki, H.-J. Galla, and J. Wegener, Biosens. Bioelectron. **19**, 583 (2004).
[7] R. Limame, A. Wouters, B. Pauwels, E. Fransen, M. Peeters, F. Lardon, O. De Wever, and P. Pauwels, PLoS ONE **7**, e46536 (2012).
[8] L. Yang, L. R. Arias, T. S. Lane, M. D. Yancey, and J. Mamouni, Anal. Bioanal. Chem. **399**, 1823 (2011).
[9] I. Giaever and C. R. Keese, Proc. Natl. Acad. Sci. USA **88**, 7896 (1991).
[10] D. C. Lovelady, T. C. Richmond, A. N. Maggi, C.-M. Lo, and D. A. Rabson, Phys. Rev. E **76**, 041908 (2007).
[11] J. H. T. Luong, Anal. Lett. **36**, 3147 (2003).
[12] M. Marimuthu, C. Park, S. Kim, and C. S. Choi, Int. J. Nanomed. **7**, 83 (2012).
[13] P. K. Mattila and P. Lappalainen, Nat. Rev. Mol. Cell Biol. **9**, 446 (2008).
[14] L. M. Machesky, FEBS Lett. **582**, 2102 (2008).
[15] M. Yilmaz and G. Christofori, Cancer Metastasis Rev. **28**, 15 (2009).
[16] P. Friedl and K. Wolf, Nat. Rev. Cancer **3**, 362 (2003).
[17] H. Yamaguchi, J. Wyckoff, and J. Condeelis, Curr. Opin. Cell Biol. **17**, 559 (2005).
[18] C.-T. Yang, R. Méjard, H. J. Griesser, P. O. Bagnaninchi, and B. Thierry, Anal. Chem. **87**, 1456 (2015).
[19] B. Hinz, W. Alt, C. Johnen, V. Herzog, and H.-W. Kaiser, Exp. Cell Res. **251**, 234 (1999).
[20] K. K. Parker, A. L. Brock, C. Brangwynne, R. J. Mannix, N. Wang, E. Ostuni, N. A. Geisse, J. C. Adams, G. M. Whitesides, and D. E. Ingber, FASEB J. **16**, 1195 (2002).
[21] M. Tarantola, A.-K. Marel, E. Sunnick, H. Adam, J. Wegener, and A. Janshoff, Integr. Biol. **2**, 139 (2010).
[22] Z. Wang, J. Kiely, M. Nibouche, and R. W. Luxton, in *Proceedings of the 10th World Congress on Biosensors, Shanghai, China* (Elsevier, Amsterdam, 2008), pp. 1–4.
[23] Y.-T. Lai and C.-M. Lo, in *Engineering in Medicine and Biology Society (EMBC), 2014 36th Annual International Conference of the IEEE* (IEEE, USA, 2014), pp. 3200–3203.
[24] S.-W. Chen, J. M. Yang, J.-H. Yang, S. J. Yang, and J.-S. Wang, Biosens. Bioelectron. **33**, 196 (2012).
[25] D. B. Percival and A. T. Walden, *Wavelet Methods for Time Series Analysis* (Cambridge University Press, Cambridge, 2000).
[26] R. C. Gonzalez, *Digital Image Processing* (Pearson Education, India, 2009).
[27] R. M. Neve, K. Chin, J. Fridlyand, J. Yeh, F. L. Baehner, T. Fevr, L. Clark, N. Bayani, J.-P. Coppe, F. Tong *et al.*, Cancer Cell **10**, 515 (2006).
[28] P. Boukamp, R. T. Petrussevska, D. Breitkreutz, J. Hornung, A. Markham, and N. E. Fusenig, J. Cell Biol. **106**, 761 (1988).
[29] A. Hall, Science **279**, 509 (1998).
[30] G. Jacquemet, H. Hamidi, and J. Ivaska, Curr. Opin. Cell Biol. **36**, 23 (2015).
[31] G. M. Nagaraja, M. Othman, B. P. Fox, R. Alsaber, C. M. Pellegrino, Y. Zeng, R. Khanna, P. Tamburini, A. Swaroop, and R. P. Kandpal, Oncogene **25**, 2328 (2005).
[32] J. W. Shay, Y. Zou, E. Hiyama, and W. E. Wright, Hum. Mol. Genet. **10**, 677 (2001).